

LONGITUDINAL OSCILLATIONS IN DENSITY STRATIFIED AND EXPANDING SOLAR WAVEGUIDES

M. LUNA-CARDOZO^{1,2}, G. VERTH³, AND R. ERDÉLYI²*Draft version March 2, 2013*

ABSTRACT

Waves and oscillations can provide vital information about the internal structure of waveguides they propagate in. Here, we analytically investigate the effects of density and magnetic stratification on linear longitudinal magnetohydrodynamic (MHD) waves. The focus of this paper is to study the eigenmodes of these oscillations. It is our specific aim to understand what happens to these MHD waves generated in flux tubes with non-constant (e.g., expanding or magnetic bottle) cross-sectional area and density variations. The governing equation of the longitudinal mode is derived and solved analytically and numerically. In particular, the limit of the thin flux tube approximation is examined. The general solution describing the slow longitudinal MHD waves in an expanding magnetic flux tube with constant density is found. Longitudinal MHD waves in density stratified loops with constant magnetic field are also analyzed. From analytical solutions, the frequency ratio of the first overtone and fundamental mode is investigated in stratified waveguides. For small expansion, a linear dependence between the frequency ratio and the expansion factor is found. From numerical calculations it was found that the frequency ratio strongly depends on the density profile chosen and, in general, the numerical results are in agreement with the analytical results. The relevance of these results for solar magneto-seismology is discussed.

Subject headings: magnetohydrodynamics (MHD) – Sun: chromosphere – Sun: corona – Sun: oscillations – waves

1. INTRODUCTION

High-resolution imaging and spectroscopic data from the *Transitional Region and Coronal Explorer* (TRACE), *Solar and Heliospheric Observatory* (SOHO), *Solar Terrestrial Relations Observatories* (STEREO) and *Hinode* have revealed a variety of wave modes in solar magnetic structures in the solar atmosphere (see, e.g., Banerjee et al. 2007; Aschwanden 2009; Taroyan & Erdélyi 2009; De Moortel 2009; Jess et al. 2009; Mathioudakis et al. 2011). Observations of standing slow magnetohydrodynamic (MHD) waves have been reported by different authors, using SOHO/SUMER (Kliem et al. 2002; Wang et al. 2002, 2003, 2005), Yohkoh (Mariska 2005, 2006) and recently, *Hinode*/EIS (Erdélyi & Taroyan 2008). For an extensive review of the observation and modeling of standing slow magnetoacoustic waves see, e.g., Wang (2011). Coronal seismology, originally suggested by Uchida (1970), Zaitsev & Stepanov (1983), and Roberts et al. (1984), allows to obtain various physical parameters (e.g., magnetic field and density scale height) through matching the MHD theory and waves observations in the corona. The concept was proposed to be used in any magnetic structure of the Sun by Erdélyi (2006) and labeled as solar magneto-seismology. The topic was extensively reviewed with plenty of references by Andries et al. (2009) and Ruderman & Erdélyi (2009).

The theory of MHD wave propagation in magnetic structures in the solar corona has been developed by

modeling the magnetic structures as homogenous cylindrical magnetic tubes embedded within a magnetic environment (Rae & Roberts 1982; Edwin & Roberts 1983; Roberts et al. 1984). Erdélyi & Fedun (2010) generalized these analytic efforts for fully compressible twisted magnetic flux tubes. Perhaps the simplest model to study the oscillatory properties is a cylindrical flux tube in pressure balance, without the complexities of gravity, curvature, radiation, bulk motion, or heating. In this case, such modeling leads to a profile with constant pressure, density, and temperature along the tube.

However, more advanced equilibrium models have also been proposed with, e.g., dissipative effects and gravity (Mendoza-Briceño et al. 2004), and it has been found that the decay times of the standing slow modes are reduced by 10% - 20% due to gravity when compared to the non-stratified loop models. Mendoza-Briceño & Luna-Cardozo (2006) included radiative cooling and heating on the study of longitudinal oscillations in hot, isothermal coronal loops with constant coronal heating; it was found that the lack of balance between cooling and heating does not affect the shape and decay time of the oscillations.

Sigalotti et al. (2007, 2008) studied standing slow waves in hot coronal loops finding that in order to achieve the same rate of damping time as detected in the observations, compressive viscosity has to be considered along with thermal conduction. Non-isothermal profiles of longitudinal waves in hot coronal loops were examined numerically, arriving at longer periods and shorter damping times when the loop becomes more non-isothermal (Erdélyi et al. 2008; Luna-Cardozo et al. 2008).

However, the theory used in these previous studies assumed a constant magnetic field along loops. Verth & Erdélyi (2008) investigated the combined effects of magnetic and density stratification on transversal coronal loop oscillations. It was found that even a relatively

mluna@iafe.uba.ar, gary.verth@northumbria.ac.uk, robertus@sheffield.ac.uk

¹ Instituto de Astronomía y Física del Espacio, CONICET-UBA, CC. 67, Suc. 28, 1428 Buenos Aires, Argentina.

² Solar Physics and Space Plasma Research Centre (SP²RC), University of Sheffield, Hicks Building, Hounsfield Road, Sheffield S3 7RH, UK.

³ School of Computing, Engineering and Information Sciences, Northumbria University, Newcastle Upon Tyne, NE1 8ST, UK.

small coronal loop expansion can have a significant and pronounced effect on the accuracy of the plasma density scale height measurements derived from observations of loop oscillations (see, e.g., Verth et al. 2008 for observational case study). Soon after, Ruderman et al. (2008) applied the theory and found that the estimated coronal scale height is a monotonically decreasing function of the tube expansion, while studying transverse oscillations in a coronal loop with variable circular cross-sectional area and plasma density in the longitudinal direction.

On average, the magnetic field strength is expected to decrease with height above the photosphere, although it has been very difficult to measure directly the variation of it in the corona. However, Lin et al. (2004) had made some progress using spectropolarimetry, and the results seem to confirm the decreasing with height of the magnetic field strength. It is expected that most loops should expand with height above the photosphere, since the flux tube cross-sectional area and magnetic field strength are inversely proportional. This expansion is defined here by

$$\Gamma = \frac{r_a}{r_f}, \quad (1)$$

where r_a is the radius at the apex and r_f is the radius at the footpoint (Klimchuk 2000). The loop expansion has been estimated for a number of loops, for example, Watko & Klimchuk (2000) reported mean values of 1.16 and 1.20 for nonflare and postflare EUV loops, respectively, analyzing *TRACE* data. Klimchuk (2000) measured a median value of $\Gamma \approx 1.30$ for soft X-ray loops using Yohkoh data. However, potential and magnetic field extrapolation had given larger loop expansions than the observed ones. DeForest (2007) suggested a possible explanation for this based on the fact that resolutions of images have not been sufficient to actually detect coronal loop expansion. Regarding the chromosphere, it has been suggested theoretically that flux tubes must undergo significant expansion with height, the so-called magnetic canopy model, e.g., Gabriel (1976). However, to date there is little observational evidence to support this (Zhang & Zhang 2000). More recently, using the Solar Optical Telescope (SOT) on board *Hinode*, for the first time Tsuneta et al. (2008) estimated an upper bound for chromospheric area expansion in the Sun's south polar region to be a factor of 345, giving a maximum expansion factor of approximately 19 for chromospheric flux tubes.

In this paper, the governing equation of the longitudinal MHD mode is derived and solved for two representative cases modeling solar atmospheric flux tubes: an expanding magnetic flux tube with arbitrary longitudinal plasma density and a density stratified flux tube with constant magnetic field. We examine the governing wave equation within the limit of the thin flux tube approximation. The slow mode is decoupled from the other MHD modes, in a similar way as applied by Díaz & Roberts (2006), where the slow mode was studied in density-structured coronal loops with constant magnetic field. The purpose of this paper is to quantify the separate effects of the expansion factor Γ and density stratification. The shooting method is applied to find numerical solutions of the general wave governing equation to compare them with analytical approximations.

2. MAGNETIC FIELD EQUILIBRIUM CONFIGURATION

The magnetic field equilibrium that decreases in strength with height above the photosphere is modeled by an expanding flux tube with rotational symmetry about the z -axis in cylindrical coordinates (r, θ, z) . Neglecting curvature along the tube axis we model an expanding tube with a straight central axis, i.e., a magnetic bottle. The tube ends are frozen in a dense photospheric plasma at $z = \pm L$, and the flux tube has an arbitrary density depending on z . This expanding magnetic field in equilibrium has two components

$$\mathbf{B} = B_r(r, z)\mathbf{e}_r + B_z(r, z)\mathbf{e}_z. \quad (2)$$

Following the derivation of Verth & Erdélyi (2008) for a potential field configuration, if small expansion is assumed it is possible to obtain an explicit expression for the perpendicular distance from the tube axis to a magnetic surface with footpoint distance from the axis defined by r_f , i.e.,

$$r_0(z) \approx r_f \left\{ 1 + \frac{(1 - \Gamma^2)}{\Gamma^2} \frac{[\cosh(z/L) - \cosh(1)]}{1 - \cosh(1)} \right\}^{-1/2} \quad (3)$$

Note that in the thin tube approximation Equation (3) is only a function of z . Similarly, the magnetic field components B_r and B_z at near the tube axis can also be described explicitly as a function of z ,

$$B_r(z) \approx -B_{z,f} \left[\frac{(1 - \Gamma^2)}{2\Gamma^2} \frac{\sinh(z/L)}{1 - \cosh(1)} \frac{r_0(z)}{L} \right] \quad (4)$$

and

$$B_z(z) \approx B_{z,f} \left\{ 1 + \frac{(1 - \Gamma^2)}{\Gamma^2} \frac{[\cosh(z/L) - \cosh(1)]}{1 - \cosh(1)} \right\}. \quad (5)$$

Therefore, B_r and B_z are related by,

$$B_r(z) \approx -\frac{1}{2}r_0(z)\frac{dB_z}{dz}. \quad (6)$$

3. GOVERNING EQUATIONS

The ideal MHD equations are linearized by assuming small magnetic perturbations $\mathbf{b} = (b_r, 0, b_z)$ and velocity perturbations $\mathbf{v} = (v_r, 0, v_z)$ about a plasma in static equilibrium. In the derivation we neglect gravity and assume constant kinetic plasma pressure. Note this means along our model of solar flux tubes that the plasma is not isothermal and the assumption of constant plasma pressure has greater validity in the corona than in the chromosphere.

Following, e.g., Roberts & Webb (1978), Roberts (2006), and Díaz & Roberts (2006), we also neglect the effect of the external environment on the perturbations, i.e., we assume the tube is in a quiescent environment. This means we do not consider any external forces acting on the tube. Inclusion of such effects is essential in the studies of, e.g., p -mode absorption of photospheric flux tubes (see Bogdan et al. 1996). The resulting MHD

conservation laws are

$$\rho_0 \frac{\partial v_r}{\partial t} = -\frac{\partial P_T}{\partial r} + \frac{1}{\mu} \left(B_r \frac{\partial b_r}{\partial r} + B_z \frac{\partial b_r}{\partial z} \right) + \frac{1}{\mu} \left(b_r \frac{\partial B_r}{\partial r} + b_z \frac{\partial B_r}{\partial z} \right), \quad (7)$$

$$\rho_0 \frac{\partial v_z}{\partial t} = -\frac{\partial P_T}{\partial z} + \frac{1}{\mu} \left(B_r \frac{\partial b_z}{\partial r} + B_z \frac{\partial b_z}{\partial z} \right) + \frac{1}{\mu} \left(b_r \frac{\partial B_z}{\partial r} + b_z \frac{\partial B_z}{\partial z} \right), \quad (8)$$

$$\frac{\partial b_r}{\partial t} = \frac{\partial}{\partial z} (B_z v_r - B_r v_z), \quad (9)$$

$$\frac{\partial b_z}{\partial t} = -\frac{1}{r} \frac{\partial}{\partial r} [r(B_z v_r - B_r v_z)], \quad (10)$$

$$\frac{\partial p}{\partial t} = -\gamma p_0 \frac{1}{r} \frac{\partial (r v_r)}{\partial r} - \gamma p_0 \frac{\partial v_z}{\partial z}, \quad (11)$$

$$P_T = p + \frac{b_r B_r}{\mu} + \frac{b_z B_z}{\mu}, \quad (12)$$

and

$$\frac{1}{r} \frac{\partial}{\partial r} (r b_r) + \frac{\partial b_z}{\partial z} = 0, \quad (13)$$

where t is time, r and z are the radial and longitudinal coordinates in the tube, ρ_0 is the plasma mass density in equilibrium, P_T is the total perturbation to pressure, p is the kinetic pressure perturbation, p_0 is the kinetic plasma pressure in equilibrium, B_r and B_z are the background components of the magnetic field, γ is the ratio of specific heats, and μ is the magnetic permeability.

3.1. Magnetic Flux Tube Equilibrium

The potential magnetic field configuration chosen in Section 2 and our choice of constant plasma pressure put restrictions on the possible types of flux tube equilibria we can model. It is always assumed that the external magnetic field is balanced by the internal one, therefore the flux tube models are not in a magnetic field free environment. Then, our assumption of constant plasma pressure demands that a flux tube with greater internal plasma density than external one must also be cooler than its environment. On the other hand, if the tube is less dense than its environment, the internal temperature must be hotter than the external.

3.2. Velocity Wave Equation

Implementing the thin tube approximation we introduce the spatial and temporal scalings $r = \epsilon R$, $z = Z$ and $t = \tau$, where $\epsilon \ll 1$. We show the details of our derivation for the governing thin tube v_z velocity equation in Appendix A. Let us introduce the following Fourier decomposition $v_z(Z, \tau) = v_z(Z) \exp(-i\omega\tau)$, where ω is the angular frequency of the oscillations. Then, the second-order ordinary differential equation for the longitudinal velocity wave is

$$\frac{d^2 v_z}{dZ^2} + f_1(Z) \frac{dv_z}{dZ} + \left[\frac{\omega^2}{c_T^2} + f_2(Z) \right] v_z = 0, \quad (14)$$

where

$$f_1(Z) = \left(\frac{c_s^2 - c_A^2}{c_T^2} \right) \frac{1}{B_z} \frac{\partial B_z}{\partial Z},$$

and

$$f_2(Z) = -\frac{1}{B_z} \frac{\partial^2 B_z}{\partial Z^2} - \left(\frac{c_s^2 - c_A^2}{c_T^2} \right) \frac{1}{B_z^2} \left(\frac{\partial B_z}{\partial Z} \right)^2.$$

For constant magnetic field, Equation (14) reduces to

$$\frac{d^2 v_z}{dZ^2} + \left(\frac{\omega^2}{c_T^2} \right) v_z = 0, \quad (15)$$

for

$$\frac{\omega^2}{c_T^2} = \omega^2 \rho_0 \left[\frac{\mu}{B_z^2} + \frac{1}{\gamma p_0} \right], \quad (16)$$

where the density may depend on Z . This equation (15) agrees with the equation obtained by Díaz & Roberts (2006), where B_z was considered constant. The solutions to Equation (15) will depend on the functional form chosen for ρ_0 in Equation (16).

3.2.1. Slow Modes in a Homogeneous Tube

For checking the derivations, we may recover the findings for a homogeneous tube (e.g., Edwin & Roberts 1983). In a straight magnetic flux tube with constant density, the solutions to Equation (15) are simply trigonometric functions. Applying the line-tying boundary at the ends of the tube, $v_z(\pm L) = 0$, we find the frequencies of the even modes given by

$$\omega_n^e = \frac{c_T}{L} \frac{(2n-1)\pi}{2}, n = 1, 2, \dots \quad (17)$$

whereas the odd modes have frequencies given by

$$\omega_n^o = \frac{c_T}{L} n\pi, n = 1, 2, \dots \quad (18)$$

The ratio of frequencies of the first overtone and fundamental mode is equal to 2, as expected.

4. ANALYTICAL SOLUTION FOR A SMOOTH DENSITY PROFILE

Since we are using cylindrical coordinates we model a solar coronal loop by a straight axisymmetric magnetic flux tube. Therefore we neglect the effect of flux tube curvature and are simply modeling the effect of gravitationally stratified plasma in a coronal loop which would produce a density profile symmetric about the loop apex. The tube length is $2L$ and its radius is r_0 . The plasma is permeated by a uniform magnetic field \mathbf{B} directed along the tube axis, $\mathbf{B} = B_z \hat{\mathbf{z}}$. The plasma density, $\rho_0(Z)$, is greater at the loop footpoints than at the apex so this is approximated by the function

$$\rho_0(Z) = \frac{\rho_a}{[1 - (1 - \kappa_1)(Z/L)^2]^2}, \quad (19)$$

where $\rho_a = \rho_0(0)$ and $\rho_f = \rho_0(\pm L)$ are the apex and footpoint densities, respectively, and $\kappa_1 = (\rho_a/\rho_f)^{1/2}$ the stratification parameter. The solid line in Figure 1 shows this smooth density profile as a function of Z . In Section 7, we choose a more applicable and realistic exponential density profile and solve Equation (15) numerically. However, the choice of density given by Equation (19) allows us to have a straightforward analytical insight into the effect of density stratification on longitudinal oscillations.

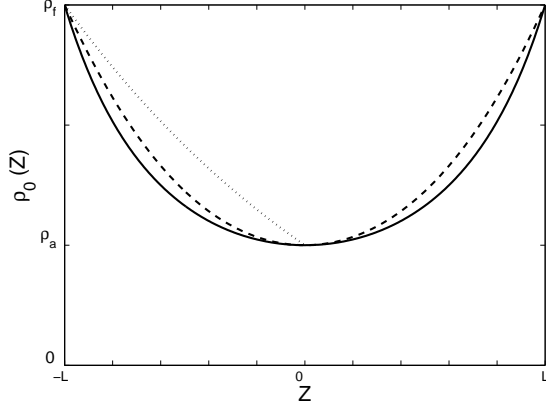


FIG. 1.— Density profile of the loop. The solid line shows the smooth density profile (19) while the dashed line shows the exponential density profile of a coronal loop (44), and the dotted line shows the exponential density profile of a chromospheric flux tube (46).

With the equilibrium density profile given by Equation (19), Equation (15) takes the form

$$\frac{d^2 v_z}{dZ^2} + \frac{\omega^2}{c_{T,a}^2} \frac{1}{[1 - (1 - \kappa_1)(Z/L)^2]^2} v_z = 0, \quad (20)$$

for $c_{T,a} = c_T(0)$, the tube speed at the apex. The general solution of this equation is (see Polyanin & Zaitsev 2003)

$$v_z = \sqrt{1 - (1 - \kappa_1)(Z/L)^2} (C_1 \cos(u) + C_2 \sin(u)), \quad (21)$$

where C_1 and C_2 are arbitrary constants, and

$$u = \frac{1}{2} \sqrt{\frac{\omega^2 L^2}{c_{T,a}^2 (1 - \kappa_1)} - 1} \left(\ln \frac{L + \sqrt{1 - \kappa_1} Z}{L - \sqrt{1 - \kappa_1} Z} \right). \quad (22)$$

To study a standing wave the boundary conditions $v_z(\pm L) = 0$ are applied, and are satisfied when either $C_2 = 0$ and $\cos[u(L)] = 0$, or $C_1 = 0$ and $\sin[u(L)] = 0$. The first condition corresponds to even modes, and the second to odd modes. The frequencies of the even modes are given by

$$(\omega_n^e)^2 = \frac{(1 - \kappa_1) c_{T,a}^2}{L^2} \times \left[(2n - 1)^2 \pi^2 \left(\ln \frac{1 + \sqrt{1 - \kappa_1}}{1 - \sqrt{1 - \kappa_1}} \right)^{-2} + 1 \right], \quad (23)$$

for $n = 1, 2, \dots$, while the odd modes have frequencies given by

$$(\omega_n^o)^2 = \frac{(1 - \kappa_1) c_{T,a}^2}{L^2} \times \left[(2n\pi)^2 \left(\ln \frac{1 + \sqrt{1 - \kappa_1}}{1 - \sqrt{1 - \kappa_1}} \right)^{-2} + 1 \right], \quad (24)$$

for $n = 1, 2, \dots$

The frequencies of the fundamental mode and the first overtone are given by Equations (23) and (24) with $n = 1$, respectively. Theoretically it is predicted that the frequencies of higher harmonics have a much stronger dependence on density stratification (e.g., Andries et al.

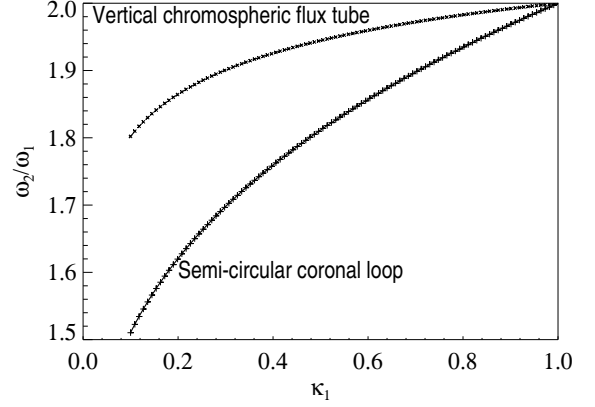


FIG. 2.— Dependence of the frequency ratio of the first overtone and fundamental mode on κ_1 , for a semi-circular coronal loop in solid line (25), and for a vertical chromospheric flux tube in dashed line (40). The “+” and “x” symbols represent the numerical solutions of Equation (20) for $Z \in [-L, L]$ and $Z \in [-L, 0]$, respectively.

2005). The ratio of frequencies of the first overtone and fundamental mode is given by

$$\frac{\omega_2}{\omega_1} = \frac{\omega_1^o}{\omega_1^e} = \left[\frac{4\pi^2 + \left(\ln \frac{1 + \sqrt{1 - \kappa_1}}{1 - \sqrt{1 - \kappa_1}} \right)^2}{\pi^2 + \left(\ln \frac{1 + \sqrt{1 - \kappa_1}}{1 - \sqrt{1 - \kappa_1}} \right)^2} \right]^{1/2}, \quad (25)$$

which is the same result obtained for the frequency ratio of the transversal mode by Dymova & Ruderman (2006). This is a remarkable property of MHD oscillations in structured waveguides. This is also rather assuring, as we arrived to these results using a completely different approach and modeling. The dependence of this ratio of frequencies on κ_1 is shown in Figure 2 by the solid line (semi-circular coronal loop). If we consider the limit of a non-stratified loop, i.e., $\kappa_1 \rightarrow 1$, we find the frequency ratio tending to 2, and it can be approximated by

$$\frac{\omega_2}{\omega_1} = 2 - \frac{3}{\pi^2} (1 - \kappa_1). \quad (26)$$

Equation (26) shows that the frequency ratio $\omega_2/\omega_1 < 2$ for a stratified loop with constant magnetic field.

5. FLUX TUBE EXPANSION WITH CONSTANT DENSITY

Let us now study the effect of magnetic stratification with a constant density on the longitudinal oscillations. For this configuration it is more convenient to use the governing pressure perturbation equation. See Appendix B for insight into the relationship between $v_z(Z)$ and $p(Z)$ when there is longitudinal stratification. The pressure wave equation (B1) with constant density is

$$\frac{d^2 p}{dZ^2} - \frac{1}{B_z} \frac{dB_z}{dZ} \frac{dp}{dZ} + \frac{\omega^2}{c_T^2} p = 0. \quad (27)$$

We can transform Equation (27) to its canonical form using the change of variable $p = P\sqrt{B_z}$. Then, Equation (27) becomes

$$\frac{d^2 P}{dZ^2} + \left[\frac{\omega^2}{c_T^2} + \frac{1}{2} \frac{1}{B_z} \frac{d^2 B_z}{dZ^2} - \frac{3}{4} \frac{1}{B_z^2} \left(\frac{dB_z}{dZ} \right)^2 \right] P = 0. \quad (28)$$

For weak magnetic stratification the ω^2/c_T^2 term has a dominant effect on the eigenvalues. To analytically investigate the behavior of the eigenvalues in this regime, we approximate Equation (28) with

$$\frac{d^2 P}{dZ^2} + \frac{\omega^2}{c_T^2} P = 0. \quad (29)$$

We suggest to use a rational function for the tube speed c_T defined by

$$c_{T,a}^2(Z) = c_{T,a}^2 \left[1 + \left(\frac{c_{T,f}}{c_{T,a}} - 1 \right) \left(\frac{Z}{L} \right)^2 \right]^2, \quad (30)$$

for $c_{T,a} = c_T(0)$ and $c_{T,f} = c_T(\pm L)$ being the apex and footpoint tube speeds, respectively. In Section 7, we solve the governing velocity equation (14) with our potential field definition of $B_z(z)$ from Equation (5) numerically. However, the choice of tube speed given by Equation (30) allows us to have a straightforward analytical insight into the effect of magnetic stratification on longitudinal oscillations.

An exact solution to Equation (29) with c_T defined by Equation (30) is given by (see Polyanin & Zaitsev 2003)

$$P = \sqrt{\alpha^2 Z^2 + 1} (C_3 \cos(\nu) + C_4 \sin(\nu)), \quad (31)$$

where C_3 and C_4 are arbitrary constants, with

$$\nu = \sqrt{\frac{\omega^2}{\alpha^2 c_{T,a}^2} + 1} \arctan(\alpha Z), \quad (32)$$

and

$$\alpha = \frac{1}{L} \sqrt{\frac{c_{T,f}}{c_{T,a}} - 1}. \quad (33)$$

In this case, to find the standing mode solution the same boundary conditions $v_z(\pm L) = P'(\pm L) = 0$ are applied. The frequencies of the even modes are given by

$$\frac{(\omega_n^e)L}{c_{T,a}} = n\pi + \left(\frac{n\pi}{3} + \frac{1}{2n\pi} \right) (\alpha L)^2 + O(\alpha L)^4, \quad (34)$$

for $n = 1, 2, \dots$, while the frequencies of the odd modes are

$$\frac{(\omega_n^o)L}{c_{T,a}} = \left(n - \frac{1}{2} \right) \pi + \left(\frac{(n - \frac{1}{2})\pi}{3} + \frac{1}{2(n - \frac{1}{2})\pi} \right) (\alpha L)^2 + O(\alpha L)^4, \quad (35)$$

for $n = 1, 2, \dots$. The ratio of frequencies of the first overtone and fundamental mode is

$$\frac{\omega_2}{\omega_1} = \frac{\omega_1^e}{\omega_1^o} = 2 - \frac{3}{\pi^2} (\alpha L)^2 + O(\alpha L)^4. \quad (36)$$

We now want to see how the effect of Γ is related to plasma β . Since we have not defined Γ explicitly in Equation (30), we combine this definition of tube speed with our potential magnetic field of $B_z(z)$ given by Equation (5), which results in the ratio of tube speeds,

$$\frac{c_{T,f}}{c_{T,a}} = \left[\frac{2 + \gamma \beta_f \Gamma^4}{2 + \gamma \beta_f} \right]^{1/2}, \quad (37)$$

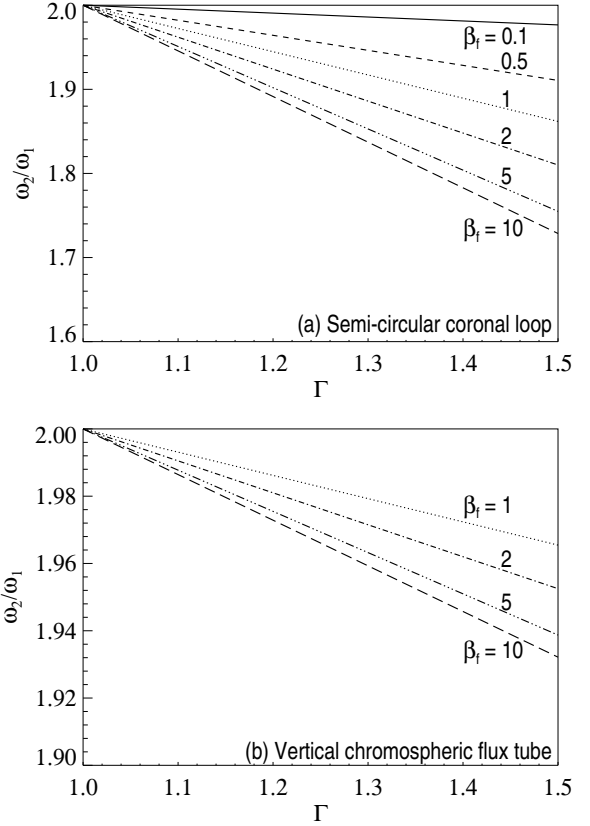


FIG. 3.— Dependence of the ratio of frequencies of the first overtone and fundamental mode (Equations (38) and (43)) on the expansion parameter Γ for different values of β_f . Solid, dashed, dotted, dot-dashed, triple-dot-dashed, and long-dashed lines correspond to $\beta_f = 0.1, 0.5, 1, 2, 5$, and 10 , respectively.

where $\beta_f = 2\mu p_0/B_{z,f}^2$ is the beta plasma at the footpoints. Therefore, Equation (36) shows that change in frequency ratio is dependent only on the loop expansion factor Γ for any finite beta plasma.

If we consider the limit of a non-expanding loop, i.e., $\Gamma \sim 1$, we recover a constant tube speed along the loop. The ratio of frequencies can be Taylor expanded for $\Gamma \sim 1$ and $\gamma = 5/3$, giving

$$\frac{\omega_2}{\omega_1} = 2 - \frac{30\beta_f}{(6 + 5\beta_f)\pi^2} (\Gamma - 1). \quad (38)$$

Equation (38) clearly shows that $\omega_2/\omega_1 < 2$ for oscillations in an expanding magnetic flux tube with constant density, and it shows a clearly linear dependence with the expansion factor. This relationship between ω_2/ω_1 and Γ is shown in Figure 3(a). It is clear that increasing the magnetic stratification takes to a lower frequency ratio, and this effect is more significant for plasmas with higher β_f .

6. APPLICATION TO SOLAR PHYSICS

Our results are relevant to magneto-seismology, e.g., estimating the coronal density scale height by using the observed ratio of the fundamental frequency and first overtone of longitudinal loop oscillations.

6.1. Application to the Corona

In the solar corona the thermal pressure is generally smaller than the magnetic pressure, giving a plasma β parameter $\ll 1$. Stratified coronal loops ($0 < \kappa_1 < 1$) with constant magnetic field give a frequency ratio lower than 2 (Equation (26)).

For a 1 MK average corona, the expected hydrostatic scale height H should be about 50 Mm, therefore for any coronal loop with length of the order of H or less could be approximated by the configuration in Section 5, where the density is constant inside the loop and the tube speed (i.e., geometry of the magnetic field) is given by Equation (30).

For a very small beta plasma (i.e., $0.01 < \beta < 0.1$) the expansion has a weak effect on the frequency ratio, as it can be seen in Figure 3(a) for the solid line. The frequency ratio can be Taylor expanded for a very small plasma β_f parameter ($\beta_f \ll 1$), giving

$$\frac{\omega_2}{\omega_1} = 2 - \frac{5}{4} \left(\frac{\Gamma^4 - 1}{\pi^2} \right) \beta_f. \quad (39)$$

Equation (39) shows that $\omega_2/\omega_1 < 2$ for an expanding magnetic flux tube ($\Gamma > 1$) in the corona with constant density.

6.2. Lower Solar Atmosphere

We now calculate the frequencies of standing modes in an expanding chromospheric ($\beta > 1$) flux tube with fixed boundaries at the photosphere and transition region, since, e.g., Fujimura & Tsuneta (2009) have recently obtained observational evidence of such waves. Note that it could be possible that flux tubes undergo large expansions in the chromosphere (e.g., Tsuneta et al. 2008), so our assumption of weak magnetic stratification may have limitations in application to chromospheric wave observations. However, the size of corrections to eigenfrequencies if larger flux tube expansions are considered are as of yet still unquantified and must be the focus of a future study. Regarding our current model, to calculate the eigenfrequencies of a vertical chromospheric weakly expanding flux tube, we need to solve the eigenvalue problem in only half of our magnetic bottle, and therefore, the boundary conditions $v_z(-L) = 0$ and $v_z(0) = 0$ are applied.

For the loop with density stratification and constant magnetic field, it is found that $C_1 = 0$ and $\sin[u(-L)] = 0$ for any arbitrary constant C_2 . The frequencies for all odd and even modes (ω_n) are given by Equation (24). The frequencies of the fundamental mode and the first overtone are given by Equation (24) with $n = 1$ and 2, respectively. The ratio of frequencies of the first overtone and fundamental mode is

$$\frac{\omega_2}{\omega_1} = \frac{\left[16\pi^2 + \left(\ln \frac{1-\sqrt{1-\kappa_1}}{1+\sqrt{1-\kappa_1}} \right)^2 \right]^{1/2}}{\left[4\pi^2 + \left(\ln \frac{1-\sqrt{1-\kappa_1}}{1+\sqrt{1-\kappa_1}} \right)^2 \right]}. \quad (40)$$

It is important to note, that the value of ω_2/ω_1 strongly depends on which functional form is chosen for the equilibrium density. Figure 2 shows a comparison of the dependence of the frequency ratios on the parameter κ_1 , in the lower atmosphere (dashed line) and in the corona (solid line). When we consider the limit of a non-stratified loop, i.e., $\kappa_1 = 1$, we recover the ratio of fre-

quencies equal to 2. Equation (40) can be approximated to

$$\frac{\omega_2}{\omega_1} = 2 - \frac{3}{4\pi^2} (1 - \kappa_1), \quad (41)$$

for $\kappa_1 \sim 1$. Equation (41) shows that the frequency ratio $\omega_2/\omega_1 < 2$ for a stratified loop ($\kappa_1 < 1$) in the lower solar atmosphere. Note that for our coronal loop model the densities at both tube ends are equal with the density profile symmetric about the apex. In our vertical chromospheric flux tube model the densities at both ends are not equal, and the density is monotonically decreasing as a function of height. It is found that the effect of the density stratification on the frequency ratio is larger in the corona than in the lower atmosphere, due to the asymmetric nature of the density profile in the chromosphere.

In the second case, a loop with magnetic stratification and constant density, the same boundary conditions are applied. The frequencies for all odd and even modes (ω_n) are given by Equation (34).

The ratio of frequencies of the first overtone and fundamental mode is

$$\frac{\omega_2}{\omega_1} = 2 - \frac{3}{4\pi^2} (\alpha L)^2 + O(\alpha L)^4. \quad (42)$$

The Taylor expansion of Equation (42) for $\Gamma \sim 1$ is

$$\frac{\omega_2}{\omega_1} = 2 - \frac{15}{2} \frac{\beta_f}{(6 + 5\beta_f)\pi^2} (\Gamma - 1), \quad (43)$$

showing again that $\omega_2/\omega_1 < 2$ and it has a linear dependence on Γ for standing waves in the lower atmosphere with constant density and weak magnetic expansion. This frequency ratio as a function of Γ is shown in Figure 3(b). The effect of the magnetic stratification on the frequency ratio is smaller in the lower solar atmosphere than in the corona.

7. NUMERICAL SOLUTIONS

In this section, we compare the analytical approximate solutions with the numerical solution of Equation (14), using the shooting method based on the Runge-Kutta technique.

7.1. Stratified Loop with Constant Magnetic Field

Equation (14) becomes Equation (15) when B_z is constant. Equation (15) can be solved numerically for both a semi-circular coronal loop and a vertical chromospheric flux tube, depending on the equilibrium chosen.

In the first case, for a semi-circular coronal loop perpendicular to the plane of the photosphere with $z \in [-L, L]$, the density is defined by (see dashed line of Figure 1)

$$\rho_0(z) = \rho_f \exp \left[-\frac{2L}{\pi H} \cos \left(\frac{\pi z}{2L} \right) \right], \quad (44)$$

where H is the density scale height and ρ_f the footpoint density. Hence, in this case the parameter κ_1 of Section 4 is a function of H and is given by

$$\kappa_1^2 = \exp \left(-\frac{2L}{\pi H} \right). \quad (45)$$

The frequency ratio obtained with the density profile (44) as a function of κ_1 is shown in Figure 4 by the solid line.

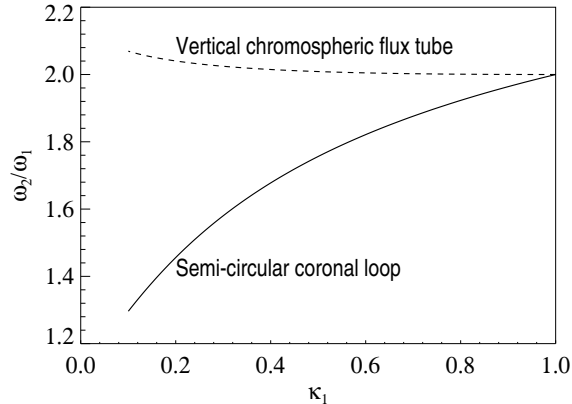


FIG. 4.— Dependence of the ratio of frequencies of the first overtone and fundamental mode on κ_1 , for a semi-circular coronal loop in solid line (44) and for a vertical chromospheric flux tube in dashed line (46), obtained from the numerical calculations.

It is clearly lower than 2, similar to the results obtained in the analytical case.

For a vertical chromospheric flux tube with $z \in [-L, 0]$, the density profile shown by the dotted line in Figure 1 is

$$\rho_0(z) = \rho_f \exp \left[-\frac{(z+L)}{H} \right], \quad (46)$$

where the parameter κ_1 is now given by

$$\kappa_1^2 = \exp \left(-\frac{L}{H} \right). \quad (47)$$

Equation (15) with density profile given by Equation (46) has the well-known solution

$$v_z(Z) = C_5 J_0 \left(\frac{2H\omega}{c_T(Z)} \right) + C_6 Y_0 \left(\frac{2H\omega}{c_T(Z)} \right), \quad (48)$$

where C_5 and C_6 are arbitrary constants. To find the eigenvalues using solution (48), we must solve a transcendental equation by either analytical or numerical techniques. Here, we choose to solve it numerically. See, e.g., McEwan et al. (2008) and Verth et al. (2010) for analytical solutions of equivalent equations in their studies of other MHD waves in limiting cases of weak stratification for both coronal loop and vertical flux tube geometries.

The dependence of the ratio of frequencies on κ_1 for the density profile (46) is shown in Figure 4 by the dashed line. In this case, the frequency ratio is greater than 2, confirming that this parameter strongly depends on the choice of the functional form of density. This means that caution must be used when interpreting the frequency ratio of chromospheric standing modes. For example, the choice of a density profile that gives a tube speed increasing linearly with height results in $\omega_2/\omega_1 < 2$, while the choice of a density profile giving a tube speed exponentially increasing with height gives $\omega_2/\omega_1 > 2$.

7.2. Expanding Loop with Constant Density

Using Equation (5) for $B_z(z)$ with $z \in [-L, L]$ we can now compute the numerical solution of Equation (14) for longitudinal oscillations in a coronal loop. Figure 5(a) shows the frequency ratio of the first overtone and fundamental mode as a function of the expansion parameter Γ for different values of β_f . It is found that increasing the

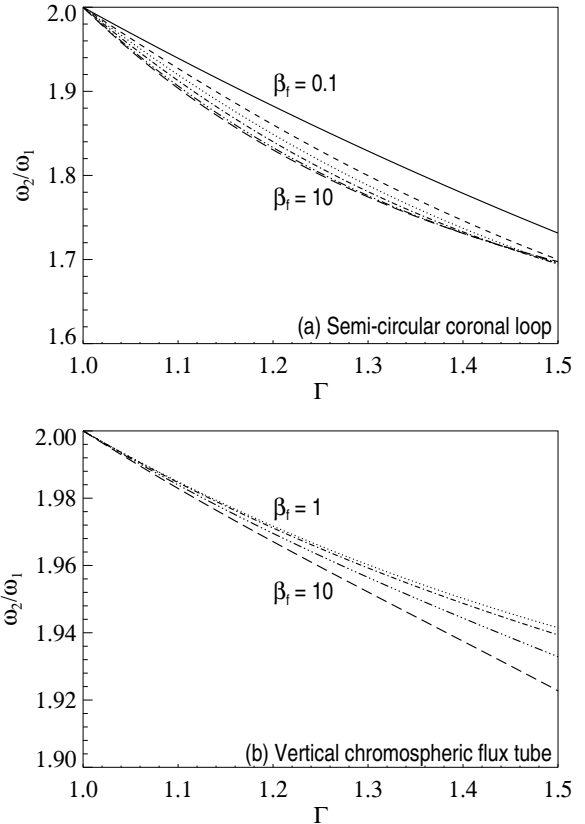


FIG. 5.— Dependence of the frequency ratio of the first overtone and fundamental mode on the expansion parameter Γ for different values of β_f obtained from the numerical calculations. Solid, dashed, dotted, dot-dashed, triple-dot-dashed, and long-dashed lines correspond to $\beta_f = 0.1, 0.5, 1, 2, 5$, and 10 , respectively.

magnetic stratification leads to a lower frequency ratio, and this effect is more significant for solar waveguides with higher β_f . These results are very similar to the results obtained in the analytical analysis.

To study the eigenmodes of a vertical chromospheric flux tube, we use Equation (5) for $B_z(z)$ with $z \in [-L, 0]$ obtaining the numerical solution of Equation (14). The dependence of the frequency ratio of the first overtone and fundamental mode on the expansion parameter is shown in Figure 5(b). The effects of the expansion Γ is somewhat smaller in the chromosphere than in the corona, being consistent with the analytical results. Also, the values of the frequency ratio for $\Gamma < 1.5$ (weak expansion) obtained from numeric and analytical calculations are very similar.

8. IMPLICATIONS FOR SOLAR MAGNETO-SEISMOLOGY

The governing equation (14) is valid for both density and magnetic stratification. We investigated the two effects, density and magnetic variations, on the value of ω_2/ω_1 separately for clarity in Sections 4 - 7. Now we discuss the combined effects in realistic solar waveguides where it is likely that the two types of stratification are present simultaneously.

8.1. Semi-circular Coronal Loops: Effect of both Density and Magnetic Stratification

In the case of a coronal loop, it was shown in Sections 4 and 5 analytically and Section 7 numerically, that if

there is density stratification (magnetic field constant) then $\omega_2/\omega_1 < 2$ and if there is magnetic stratification (constant density) then also $\omega_2/\omega_1 < 2$. Hence, regarding the value of ω_2/ω_1 the two effects are not competing against each other, in contrast to the kink mode (see, e.g., Verth & Erdélyi 2008; Ruderman et al. 2008). This result is robust, in particular, in the functional forms chosen for $\rho_0(Z)$ and $B_z(Z)$ as long as there is symmetry about the loop apex.

Observational claims of estimating slow mode values of ω_2/ω_1 from intensity perturbations in coronal loops have been made using both EUV (Srivastava & Dwivedi 2010) and X-ray (Kumar et al. 2011) data from *Hinode*. Srivastava & Dwivedi (2010) claim to detect two separate cases in EUV coronal loops of $\omega_2/\omega_1 < 2$. However, in these observed coronal loops the value of plasma β may be very low, and in this limit $c_T(z) \approx c_s(Z)$. In this situation it is the variation of $c_s(Z)$ in wave equation (14) that would have the dominating effect on the value of ω_2/ω_1 and magnetic stratification, even if present, would not play a significant part. Assuming the observed loops are isobaric and density is decreasing as a function of height, then even in the zero- β limit, our model gives $\omega_2/\omega_1 < 2$, consistent with these particular EUV observations. Physically, this would be due to $c_s(Z)$ increasing with height in a coronal loop, i.e., temperature hotter at the apex than at the footpoints.

Regarding the study by Kumar et al. (2011) of slow mode values of ω_2/ω_1 in X-ray small-scale loops, Table 1 of that paper shows six separate estimates of ω_2/ω_1 and one particular case of ω_3/ω_1 . Three estimates have $\omega_2/\omega_1 < 2$, similar to the measurements of Srivastava & Dwivedi (2010), but in contrast three also have $\omega_2/\omega_1 > 2$. In the low- β limit, the observations of $\omega_2/\omega_1 > 2$, could be explained by $c_s(Z)$ decreasing as a function of height in these loops, i.e., the temperature being hotter at foot-points than at the apex. However, to explain this our isobaric model would require density increasing with height to have $c_s(Z)$ decreasing with height and this is unphysical. To model such a coronal loop more realistically, one would also need to model $p(Z)$ and choose $\rho(Z)$ such that temperature is hotter at foot-points than at apex. This would be an important future extension to this current work.

8.2. Vertical Flux Tubes: Effect of both Density and Magnetic Stratification

Our study of magnetic stratification (constant density) in vertical flux tubes resulted in $\omega_2/\omega_1 < 2$ for both the hyperbolic profile for $B_z(Z)$ given by Equation (5) and the tube speed given by the rational function in Equation (30). However, it was shown that for the case of density stratification (constant magnetic field) in a vertical flux tube, ω_2/ω_1 could either be greater or less than 2 depending on the functional form chosen. E.g., $\omega_2/\omega_1 < 2$ for the smooth rational function of density given by Equation (19) and $\omega_2/\omega_1 > 2$ for the exponential profile of $\rho_0(Z)$ given by Equation (46). In our investigation we have shown that, depending on the functional forms chosen, density stratification and magnetic stratification could both cause the value of ω_2/ω_1 to be less than 2, or the effects could oppose each other. This means that magneto-seismology for vertical flux tubes in the chromosphere may be more subtle than in the case of

coronal loops when it comes to interpreting the observed values of ω_2/ω_1 .

9. SUMMARY AND CONCLUSIONS

In this paper the effects of density and magnetic stratification on longitudinal oscillations in isobaric coronal and chromospheric conditions have been studied. Solar waveguides were modeled as axisymmetric cylindrical magnetic tubes. The governing equation were derived and solved by analytical approximation, and examined in the thin flux tube limit. We studied the effects of magnetic stratification while the density is constant and density stratification for a constant magnetic field.

From the analytic solutions, both density stratified and expanding coronal loops have $\omega_2/\omega_1 < 2$. For small expansion, a linear dependence between the frequency ratio and the expansion factor is found. It was also found that the effect of magnetic field strength decreasing with height has the same effect on the frequency ratios to that of gravitational density stratification, in contrast with the results for kink modes (Verth & Erdélyi 2008; Andries et al. 2005).

It was found that the introduction of waveguide structuring results in a modification to the oscillatory frequency of the mode. The expression for the frequency ratio obtained in Section 5 (Equation (38)) depends on the expansion parameter Γ and an additional dependence on β_f was found, due to the inclusion of kinetic pressure in our model.

Next, numerical solutions were performed. The numerical results were consistent with the analytic solutions for the coronal loop model. Also, for the vertical chromospheric flux tube model it was found that the frequency ratio strongly depends on the functional form of the density, suggesting that caution must be used when interpreting the frequency ratios of chromospheric standing modes.

The effect of gravity was neglected in the present study. It is known for propagating longitudinal waves that the cutoff frequency is increased by the inclusion of gravity (see, e.g., Roberts & Webb 1978), which introduces a Brunt-Väisälä (buoyancy) term into the governing equations. This term has been shown to be relevant for the leakage of p -mode driven longitudinal waves into the upper atmosphere (De Pontieu et al. 2004, 2005), since the influence of the Brunt-Väisälä term in the cutoff frequency can be reduced by the amount of magnetic field inclination, i.e., the more tilted the field from the vertical, the lower the effective cut-off frequency. In a future study, it would therefore be of great interest to investigate the effect of gravity and field inclination on the longitudinal standing modes, e.g., to quantify the importance of the Brunt-Väisälä (buoyancy) term on the eigenfunctions and eigenvalues.

It is important to progress the field of magneto-seismology that any proposed model can be tested against the observed oscillatory properties of solar waveguides. The theory presented in this paper should be helpful in this regard, modeling both magnetic and density stratification along solar waveguides which can be used to interpret observations of standing slow oscillations such as those by Srivastava & Dwivedi (2010) and Kumar et al. (2011). In the future, it will also be beneficial to find the solutions of the governing equation when stronger

magnetic stratification is considered.

M.L.-C. thanks the support by the University of Sheffield Fellowship, Overseas Research Students Award (ORS), and the financial support from the Argentinean

grant PICT 2007-1790 (ANPCyT). R.E. acknowledges M. K  ray for patient encouragement and is also grateful to NSF, Hungary (OTKA, Ref. No. K83133). The authors also thank R. Morton for providing guidance on the numerical results.

APPENDIX

DERIVATION OF VELOCITY WAVE EQUATION

In this Appendix we derive the velocity wave equation (14). Equations (7)-(13) may be combined to yield the general equations for v_z , v_r , and P_T ,

$$\begin{aligned} \frac{\partial}{\partial z} \left(\frac{\partial P_T}{\partial t} \right) + \left[\rho_0 \frac{\partial^2 v_z}{\partial t^2} - \frac{B_r^2}{\mu} \frac{\partial^2 v_z}{\partial r^2} - \frac{B_r B_z}{\mu} \frac{\partial^2 v_z}{\partial r \partial z} \right] + \left[-\frac{B_r}{\mu} \frac{\partial B_r}{\partial r} - \frac{B_z}{\mu} \frac{\partial B_r}{\partial z} \right] \frac{\partial v_z}{\partial r} + \left[\frac{B_z}{\mu} \frac{\partial B_z}{\partial z} + \frac{B_r}{\mu} \frac{\partial B_z}{\partial r} \right] \frac{\partial v_z}{\partial z} \\ + \left[\frac{B_r}{\mu} \frac{\partial^2 B_z}{\partial r \partial z} + \frac{1}{\mu} \frac{\partial B_z}{\partial r} \frac{\partial B_r}{\partial z} + \frac{B_z}{\mu} \frac{\partial^2 B_z}{\partial z^2} + \frac{1}{\mu} \left(\frac{\partial B_z}{\partial z} \right)^2 \right] v_z + \left[\frac{B_r B_z}{\mu} \frac{\partial^2 v_r}{\partial r^2} + \frac{B_z^2}{\mu} \frac{\partial^2 v_r}{\partial r \partial z} \right] + \frac{B_z^2}{\mu r} \frac{\partial v_r}{\partial z} \\ + \left[\frac{2B_r}{\mu} \frac{\partial B_z}{\partial r} + \frac{B_r B_z}{\mu r} + \frac{2B_z}{\mu} \frac{\partial B_z}{\partial z} \right] \frac{\partial v_r}{\partial r} + \left[\frac{B_r}{\mu r} \frac{\partial B_z}{\partial r} + \frac{B_r}{\mu} \frac{\partial^2 B_z}{\partial r^2} + \frac{B_z}{\mu} \frac{\partial^2 B_z}{\partial r \partial z} - \frac{B_r B_z}{\mu r^2} + \frac{2B_z}{\mu r} \frac{\partial B_z}{\partial z} \right] v_r = 0, \end{aligned} \quad (A1)$$

$$\begin{aligned} \frac{\partial}{\partial r} \left(\frac{\partial P_T}{\partial t} \right) + \left[\rho_0 \frac{\partial^2 v_r}{\partial t^2} - \frac{B_z^2}{\mu} \frac{\partial^2 v_r}{\partial z^2} - \frac{B_r B_z}{\mu} \frac{\partial^2 v_r}{\partial r \partial z} \right] + \left[\frac{B_z}{\mu} \frac{\partial B_r}{\partial z} - \frac{B_r}{\mu} \frac{\partial B_z}{\partial r} \right] \frac{\partial v_r}{\partial r} \\ - \left[\frac{B_r}{\mu} \frac{\partial B_z}{\partial r} + \frac{2B_z}{\mu} \frac{\partial B_z}{\partial z} + \frac{B_z}{\mu} \frac{\partial B_r}{\partial r} \right] \frac{\partial v_r}{\partial z} + \left[\frac{1}{\mu} \frac{\partial B_z}{\partial r} \frac{\partial B_r}{\partial z} - \frac{B_r}{\mu} \frac{\partial^2 B_z}{\partial r \partial z} - \frac{B_z}{\mu} \frac{\partial^2 B_z}{\partial z^2} + \frac{B_z}{\mu r} \frac{\partial B_r}{\partial z} - \frac{1}{\mu} \frac{\partial B_r}{\partial r} \frac{\partial B_z}{\partial z} \right] v_r \\ + \left[\frac{B_r^2}{\mu} \frac{\partial^2 v_z}{\partial r \partial z} + \frac{B_r B_z}{\mu} \frac{\partial^2 v_z}{\partial z^2} \right] + \left[\frac{2B_r}{\mu} \frac{\partial B_r}{\partial r} + \frac{2B_z}{\mu} \frac{\partial B_r}{\partial z} \right] \frac{\partial v_z}{\partial z} + \left[\frac{B_r}{\mu} \frac{\partial^2 B_r}{\partial r \partial z} + \frac{B_z}{\mu} \frac{\partial^2 B_r}{\partial z^2} - \frac{B_r}{\mu r} \frac{\partial B_r}{\partial z} \right] v_z = 0, \end{aligned} \quad (A2)$$

$$\begin{aligned} \frac{\partial P_T}{\partial t} = -\frac{B_z^2}{\mu} \left(\frac{\partial v_r}{\partial r} + \frac{v_r}{r} \right) - \gamma p_0 (\nabla \cdot \mathbf{v}) + \left(\frac{B_r B_z}{\mu} \frac{\partial v_z}{\partial r} - \frac{B_r^2}{\mu} \frac{\partial v_z}{\partial z} \right) \\ - \left(\frac{B_r}{\mu} \frac{\partial B_r}{\partial z} + \frac{B_z}{\mu} \frac{\partial B_z}{\partial z} \right) v_z + \frac{B_r B_z}{\mu} \frac{\partial v_r}{\partial z} + \left(\frac{B_r}{\mu} \frac{\partial B_z}{\partial z} - \frac{B_z}{\mu} \frac{\partial B_r}{\partial r} \right) v_r, \end{aligned} \quad (A3)$$

If we compare Equations (A1)-(A3) with Equations (1)-(3) from D  az & Roberts (2006, who studied density stratification with a constant magnetic field), the added complexity to the governing wave equations if we have an equilibrium with an expanding magnetic field can readily be appreciated.

Here we are interested in the behavior of slow magnetoacoustic modes, we introduce the following spatial and temporal scalings:

$$r = \epsilon R, \quad z = Z, \quad v_r = \epsilon v_R, \quad v_z = v_z, \quad B_r = \epsilon B_R, \quad B_z = B_z, \quad \text{and} \quad t = \tau. \quad (A4)$$

It is interesting to note that such scaling have been used in the analysis of slow modes within resonant layers in a magnetically structured plasma (e.g., Ballai et al. 1998) and to study slow MHD waves in a stratified medium (e.g., Roberts 2006, except that in his study the stretching was only on the position and time since the magnetic field was considered constant).

Considering the thin tube approximation, $\epsilon \ll 1$, i.e., the r -coordinate has a small range in comparison with the z -coordinate. Since we are interested in the longitudinal component of the wave, we focus on the equation of v_z , and after the scaling it becomes

$$\begin{aligned} \rho_0 \left[\frac{\partial^2 v_z}{\partial \tau^2} - c_T^2 \frac{\partial^2 v_z}{\partial Z^2} \right] - \frac{c_s^2}{c_f^2} \frac{B_R^2}{\mu} \frac{\partial^2 v_z}{\partial R^2} - \frac{c_s^2}{c_f^2} \frac{2B_R B_z}{\mu} \frac{\partial^2 v_z}{\partial R \partial Z} + \left[\left(\frac{c_T^2}{c_f^2} - \frac{c_s^4}{c_f^4} \right) \frac{B_z}{\mu} \frac{\partial B_z}{\partial Z} \right] \frac{\partial v_z}{\partial Z} \\ + \left[\frac{c_T^2}{c_f^2} \frac{2B_R}{\mu} \frac{\partial B_z}{\partial Z} - \frac{c_s^2}{c_f^2} \left(\frac{B_R}{\mu} \frac{\partial B_R}{\partial R} + \frac{B_z}{\mu} \frac{\partial B_R}{\partial Z} \right) \right] \frac{\partial v_z}{\partial R} + \left[\frac{c_s^2}{c_f^2} \frac{B_z}{\mu} \frac{\partial^2 B_z}{\partial Z^2} + \left(\frac{c_s^4}{c_f^4} - \frac{c_T^2}{c_f^2} \right) \frac{1}{\mu} \left(\frac{\partial B_z}{\partial Z} \right)^2 \right] v_z = 0, \end{aligned} \quad (A5)$$

where $c_A = (B_z^2/\mu\rho_0)^{1/2}$ and $c_s = (\gamma p_0/\rho_0)^{1/2}$ are the Alfv  n and sound speeds, respectively. The square of the fast phase speed is defined by $c_f^2 = c_s^2 + c_A^2$ and the tube speed is given by $c_T^{-2} = c_s^{-2} + c_A^{-2}$.

The R -derivatives of perturbed quantities are very small compared with the Z -derivatives since we consider the thin tube approximation, i.e., $\partial v_z/\partial R \ll 1$.

PRESSURE WAVE EQUATION

In this Appendix, we present the governing pressure equation and the relationship between velocity and pressure amplitude for longitudinal stratification. Equations (7)-(13) may also be combined to give an equation for the (per-

turbation) pressure amplitude $p(z)$, defined by $p(z, t) = p(z) \exp(i\omega t)$. If one follows this route, one will arrive at

$$\frac{d^2 p}{dZ^2} - \left(\frac{1}{\rho_0} \frac{d\rho_0}{dZ} + \frac{1}{B_z} \frac{dB_z}{dZ} \right) \frac{dp}{dZ} + \frac{\omega^2}{c_T^2} p = 0, \quad (\text{B1})$$

after applying the same scaling as defined by (A4). Equation (B1) is consistent with the results obtained by Roberts & Webb (1978). From Equation (8), the following relation is obtained:

$$\frac{\partial p}{\partial Z} = -\rho_0(Z) \frac{\partial v_z}{\partial \tau}. \quad (\text{B2})$$

We can find the velocity amplitude equation from the pressure equation by using (B2):

$$\begin{aligned} \frac{d^2 v_z}{dZ^2} + \left(\frac{1}{c_T^2} \frac{\partial c_T^2}{\partial Z} + \frac{1}{\rho_0} \frac{\partial \rho_0}{\partial Z} - \frac{1}{B_z} \frac{\partial B_z}{\partial Z} \right) \frac{dv_z}{dZ} + \left[\frac{\omega^2}{c_T^2} - \frac{1}{B_z} \frac{\partial^2 B_z}{\partial Z^2} + \frac{1}{B_z^2} \left(\frac{\partial B_z}{\partial Z} \right)^2 \right] v_z \\ + \left[-\frac{1}{\rho_0} \frac{\partial \rho_0}{\partial Z} \frac{1}{B_z} \frac{\partial B_z}{\partial Z} - \frac{1}{c_T^2} \frac{\partial c_T^2}{\partial Z} \frac{1}{B_z} \frac{\partial B_z}{\partial Z} \right] v_z = 0, \end{aligned} \quad (\text{B3})$$

which is indeed equivalent to Equation (14) and that can be checked rather easily.

REFERENCES

- Andries, J., Arregui, I., & Goossens, M. 2005, *ApJ*, 624, L57
Andries, J., van Doorselaere, T., Roberts, B., et al. 2009, *Space Sci. Rev.*, 149, 3
Aschwanden, M. J. 2009, *Space Sci. Rev.*, 149, 31
Ballai, I., Ruderman, M. S., & Erdélyi, R. 1998, *Phys. Plasma*, 5, 252
Banerjee, D., Erdélyi, R., Oliver, R., & O'Shea, E. 2007, *Sol. Phys.*, 246, 3
Bogdan, T. J., Hindman, B. W., Cally, P. S. & Charbonneau, P. 1996, *ApJ*, 465, 406
DeForest, C. E. 2007, *ApJ*, 661, 532
De Moortel, I. 2009, *Space Sci. Rev.*, 149, 65
De Pontieu, B., Erdélyi, R. & De Moortel, I. 2005, *ApJ*, 624, L61
De Pontieu, B., Erdélyi, R. & James, S. P. 2004, *Nature*, 430, 536
Díaz, A. J., & Roberts, B. 2006, *A&A*, 458, 975
Dymova, M. V., & Ruderman, M. S. 2006, *A&A*, 457, 1059
Edwin, P. M., & Roberts, B. 1983, *Sol. Phys.*, 88, 179
Erdélyi, R. 2006, *Phil. Trans. R. Soc. A*, 364, 351
Erdélyi, R., & Fedun, V. 2010, *Sol. Phys.*, 263, 63
Erdélyi, R., Luna-Cardozo, M., & Mendoza-Briceño, C. A. 2008, *Sol. Phys.*, 252, 305
Erdélyi, R., & Taroyan, Y. 2008, *A&A*, 489, L49
Fujimura, D., & Tsuneta, S. 2009, *ApJ*, 702, 1443
Gabriel, A. H. 1976, *Phil. Trans. R. Soc. A*, 281, 339
Jess, D. B., Mathioudakis, M., Erdélyi, R., et al. 2009, *Science*, 323, 1582
Kliem, B., Dammasch, I. E., Curdt, W., & Wilhelm, K. 2002, *ApJ*, 568, L61
Klimchuk, J. A. 2000, *Sol. Phys.*, 193, 53
Kumar, M., Srivastava, A. K. & Dwivedi, B. N. 2011, *MNRAS*, 415, 1419
Lin, H., Khun, J. R., & Coulter, R. 2004, *ApJ*, 613, L177
Luna-Cardozo, M., Erdélyi, R., & Mendoza-Briceño, C. A. 2008, in *IAU Symp. 247, Waves and Oscillations in the Solar Atmosphere: Heating and Magneto-Seismology*, ed. R. Erdélyi & C. A. Mendoza-Briceño (Cambridge: Cambridge Univ. Press), 316
Mariska, J. T. 2005, *ApJ*, 620, L67
Mariska, J. T. 2006, *ApJ*, 639, 484
Mathioudakis, M., Jess, D. B., & Erdélyi, R. 2011, *Space Sci. Rev.*, submitted
McEwan, M. P., Díaz, A. J. & Roberts, B. 2008, *A&A*, 481, 819
Mendoza-Briceño, C. A., Erdélyi, R., & Sigalotti, L. Di G. 2004, *ApJ*, 605, 493
Mendoza-Briceño, C. A., & Luna-Cardozo, M. 2006, in *IAU Symp. 233, Solar Activity and its Magnetic Origin*, ed. V. Bothmer & A. A. Hady (Cambridge: Cambridge Univ. Press), 179
Polyanin, A. D., & Zaitsev, V. F. 2003, *Handbook of Exact Solutions for Ordinary Differential Equations* (Boca Raton, FL: Chapman & Hall)
Rae, I. C., & Roberts, B. 1982, *ApJ*, 256, 761
Roberts, B. 2006, *Phil. Trans. R. Soc. A*, 364, 447
Roberts, B., Edwin, P. M., & Benz, A. O. 1984, *ApJ*, 279, 857
Roberts, B., & Webb, A. R. 1978, *Sol. Phys.*, 56, 5
Ruderman, M. S., & Erdélyi, R. 2009, *Space Sci. Rev.*, 149, 199
Ruderman, M. S., Verth, G., & Erdélyi, R. 2008, *ApJ*, 686, 694
Sigalotti, L. Di G., Mendoza-Briceño, C. A., & Luna-Cardozo, M. 2007, *Sol. Phys.*, 246, 187
Sigalotti, L. Di G., Mendoza-Briceño, C. A., & Luna-Cardozo, M. 2008, in *IAU Symp. 247, Waves and Oscillations in the Solar Atmosphere: Heating and Magneto-Seismology*, ed. R. Erdélyi & C. A. Mendoza-Briceño (Cambridge: Cambridge Univ. Press), 316
Srivastava, A. K. & Dwivedi, B. N. 2010, *New Astron.*, 15, 8
Taroyan, Y., & Erdélyi, R. 2009, *Space Sci. Rev.*, 149, 229
Tsuneta, S., Ichimoto, K., Katsukawa, Y., et al. 2008, *ApJ*, 688, 1374
Uchida, Y. 1970, *PASJ*, 22, 341
Verth, G., & Erdélyi, R. 2008, *A&A*, 486, 1015
Verth, G., Erdélyi, R. & Goossens, M. 2010, *ApJ*, 714, 1637
Verth, G., Erdélyi, R. & Jess, D. 2008, *ApJ*, 687, L45
Wang, T. J. 2011, *Space Sci. Rev.*, 158, 397
Wang, T. J., Solanki, S. K., Curdt, W., Innes, D. E., & Dammasch, I. E. 2002, *ApJ*, 574, L101
Wang, T. J., Solanki, S. K., Innes, D. E., & Curdt, W. 2005, *A&A*, 435, 753
Wang, T. J., Solanki, S. K., Innes, D. E., Curdt, W., & Marsch, E. 2003, *A&A*, 402, L17
Watko, J. A., & Klimchuk, J. A. 2000, *Sol. Phys.*, 193, 77
Zaitsev, V. V., & Stepanov, A. V. 1983, *Sol. Phys.*, 88, 297
Zhang, H., & Zhang, M. 2000, *Sol. Phys.*, 196, 269